THE JOURNAL OF PHYSICAL CHEMISTRY A

 VOLUME 107, NUMBER 47, NOVEMBER 27, 2003

ARTICLES

Coherent Control of Oscillatory Excitation Transfer in Dithia-1,5[3,3]anthracenophane by a Phase-Locked Femtosecond Pulse Pair

Shin-ichiro Sato,*,† Yoshinobu Nishimura,† Yoshiteru Sakata,‡ and Iwao Yamazaki*,†

Department of Molecular Chemistry, Graduate School of Engineering, Hokkaido University, Sapporo 060-8628, Japan, and The Institute of Scientific and Industrial Research, Osaka University, Mihoga-oka Ibaraki, Osaka 567-0047, Japan

Received: November 13, 2002; In Final Form: May 15, 2003

The intramolecular electronic excitation coherence created by the first femtosecond laser pulse in a linked-anthracene dimer, dithia-1,5[3,3]-anthracenophane (DTA), was enhanced or depreciated by the interference with the second femtosecond laser pulse, which is phase-locked to the first pulse. Two anthracene rings in DTA are stacked parallel but with nearly orthogonal orientation. The interference intensity of fluorescence from DTA was measured as a function of delay time between two pulses with the optical phase angle being fixed with 0° (in-phase) or 180° (anti-phase). Two components of enhanced and depreciated oscillations appeared in the subpicosecond region as a function of the delay time, with the time periods depending on the excitation wavelength. On the basis of theoretical analysis, the two components were assigned to the sum and difference frequencies between the energy splitting of molecular eigenstates and the detuning of the laser frequency relative to the molecular electronic transition energy. The exciton splitting between the two superposition states of the local excitation was derived to be $2\beta = 35$ cm^{-1}, which is in close agreement with our previous result (29 cm^{-1}) obtained from fluorescence anisotropy decay measurement.

1. Introduction

Electronic excitation transfers have been widely studied for organized molecular systems of synthetic organic compounds[1−5] and huge biophysical systems[6−9] in which reactant molecules are arranged with close proximity and optimal orientations. The excitation transfers in these organized molecular systems, taking place on a time scale of less than 1 ps, are expected to have a coherent nature inherently since electronic and/or vibrational dephasing times are comparable to the reaction rates. The dephasing times have been mainly measured by photon-echo-type measurements. For example, electronic dephasing times of diphenylacetylene in nonpolar solvents are reported to be 120∼500 fs at room temperature.[10]

The intramolecular energy transfer of linked bichromophoric compounds is the basic subject to examine the ultrafast coherent energy transfer. Hochstrasser and co-workers[1−3] studied the coherent excitation energy transfer between two identical chromophores in 9,9′-bifluorene and 2,2′-binaphthyl in different solvents at room temperature. The anisotropy decay of transient absorption in binaphthyl exhibited a damped oscillation corresponding to the excitation recurrence between two chromophores. They analyzed the experimental data theoretically by using the Bloch equation and found that the interchromophore interaction energy (2β) is 41 cm^{-1} and electronic dephasing time (T_2') is 200 fs. Kato and Fujimura[4] theoretically analyzed the effects of statistical distributions of relative orientations between

* Correspondence should be addressed to this author: Phone 81-11-706-6607; fax 81-11-709-2037; e-mail s-sato@eng.hokudai.ac.jp.
† Hokkaido University.
‡ Osaka University.

10.1021/jp027452d CCC: $25.00
Published on Web 11/01/2003

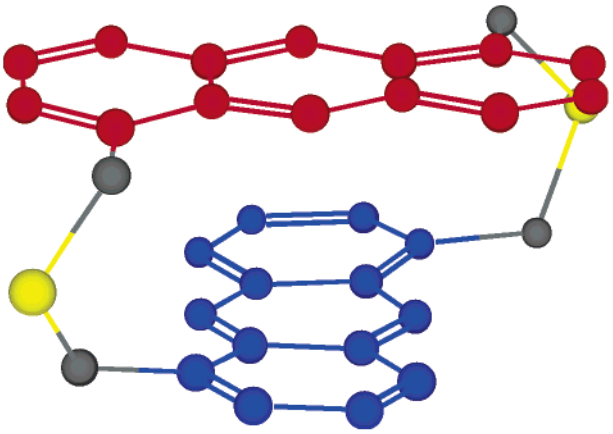

Figure 1. Molecular structure of DTA. Two anthracene rings are connected through two thioethers almost parallel with an interplane distance of 3.41 Å.

two chromophores on the beat intensities in the anisotropy measurements. Recently Yamazaki et al.[5] investigated the quantum coherence associated with pendulum motion of exciton in a linked-anthracene dimer, dithia-1,5[3,3]anthracenophane (referred to as DTA) shown in Figure 1, in tetrahydrofuran (THF) solution at room temperature by probing a damped oscillation in the time-dependent fluorescence anisotropy. In DTA, two anthracene rings are connected through two thioethers almost parallel with an interplane distance of 3.41 Å and one of the rings is rotated by 88.5° around the center of the anthracene ring.

The dimeric structure is fixed much more firmly than for the case of binaphthyl with flexible conformations.[4] An analysis of the observed oscillating signal following the theoretical equation formulated by Wynne and Hochstrasser[3] revealed that the electrostatic interaction energy between chromophores is $2\beta = 29$ cm^{-1} and the dephasing time $T_2' = 1$ ps. A fixed dimeric structure is responsible for the longer dephasing time.

We report here a coherent control experiment of the excitation energy transfer in DTA by using a phase-locked, femtosecond pulse-pair technique. The coherent control of photochemical reactions, including energy transfer, electron transfer, isomerization, and dissociation, is of considerable current interest.[11−14] The femtosecond phase-locked, pulse-pair excitation is one of the essential techniques of coherent control and has been used in combination with both linear spectroscopy (fluorescence detection)[15−18] and nonlinear spectroscopy (photon-echo detection)[19−21] to control molecular wave packets on the excited electronic potential surface.

In the phase-locked pulse-pair experiment, two photon fields, E_1 and E_2, having a fixed optical phase angle ϕ, are applied to the sample molecule. Three emission components, which are proportional to E_1^2, E_2^2, and E_1E_2, are present in the total fluorescence from the sample, and the E_1E_2 term is monitored by a dual-frequency chopped lock-in detection. The E_1E_2 term is modulated by the interference between the molecular wave packets created by E_1 and E_2 and accordingly may be enhanced or depreciated by varying the phase ϕ. Here, we present a formula representing the time evolution of the molecular wave packet generated by a phase-locked pulse-pair under nonimpulsive excitation conditions in the bichromophoric molecular system.

2. Experimental Section

2.1. Sample Preparation. Sample preparation has been described elsewhere.[22,23] Briefly, reaction of 1,5-di(methoxycarbonyl)anthracene with $LiAlH_4$ in THF, followed by bromination with PBr_3 in benzene, gave 1,5-di(bromomethyl)-anthracene. A coupling reaction with Na_2S in a mixed solvent of benzene, ethanol, and H_2O produces DTA along with oligomers. DTA was purified with silica gel chromatography. The sample of DTA, polycrystalline powder, was held between two quartz plates of 1-mm thickness and was set into a low-temperature vacuum cryostat (Daikin 202CL) maintained at 10 K during fluorescence measurements.

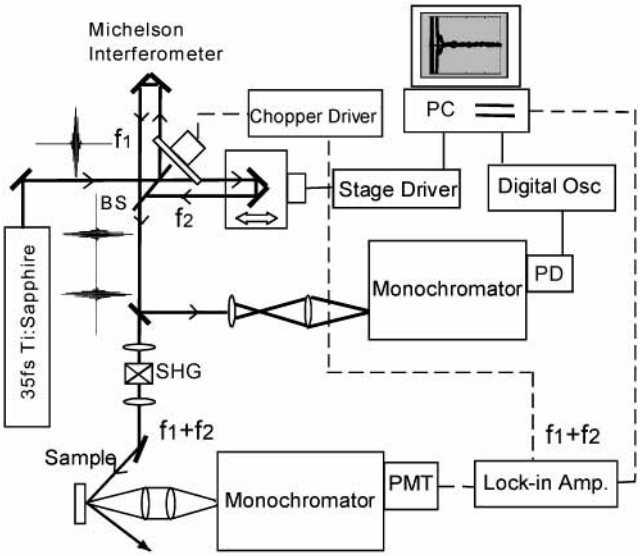

Figure 2. Schematic drawing of optical arrangement of Michelson interferometer, fringe monitor, fluorescence detection, and phase control and signal processing electronics. BS, 50% beam splitter; PMT, photomultiplier tube.

2.2. Phase-Locked Pulse-Pair Fluorescence Interferometer. Figure 2 displays a block diagram of our experimental setup. Femtosecond pulses (~40 fs, 80 MHz) from the Ti:sapphire laser (Spectra Physics Tsunami) are injected into a Michelson interferometer, the optical path length in one of whose arms is varied by a stepper-motor-driven optical delay line with 200-nm resolution, which is approximately $\lambda/4$ of the laser wavelength. A dual-frequency (f_1 and f_2) mechanical chopper, with one set of slots positioned in each arm of the interferometer, is used to modulate the cross-beam component of the total fluorescence, which is picked up through lock-in amplification referenced to the sum frequency $f_1 + f_2$. The two beams from the interferometer are recombined to propagate collinearly to maintain phase uniformity of the laser beam wave front and are frequency-doubled by a BBO crystal. Then, the double pulse excites the sample. The total fluorescence or partial fluorescence dispersed by a monochromator (Nikon P250) with a typical spectral window of 6 nm was detected by a photomultiplier tube (Hamamatsu R106) and processed by the lock-in amplifier (NF 5610B) referenced to $f_1 + f_2$.

A part of the double beam from the interferometer is reflected by a beam splitter to detect fringe intensities of the double pulse at a particular wavelength by using a monochromator (Jasco SS25C) equipped with a 1200/cm groove grating. The fringe intensity measured here is used to determine a relative optical phase angle of two beams. Figure 3 displays fringe spectra of the two beams at various time delays (t_d). Fourier transform of phase-locked double pulse, $E(t) + E(t - t_d)$, is given by the shift theorem:

$$E(t) + E(t - t_d) \xrightarrow{\text{Fourier}} E(\omega)(1 + \exp\{i\omega t_d\})$$

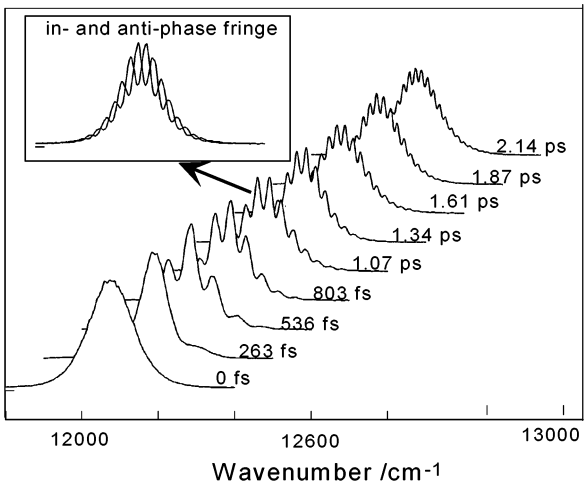

Figure 3. Fringe spectra of phase-locked double pulses at various time delays. Inset shows the relationship between in-phase and anti-phase phase locking.

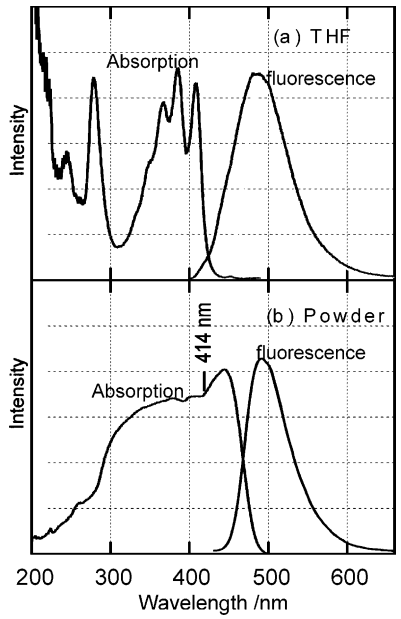

Figure 4. Fluorescence and fluorescence excitation spectra of DTA in THF solution (a) and in powder (b). Both spectra were recorded at room temperature.

where $E(\omega)$ is the Fourier transform of $E(t)$. Therefore, the interval of modulation manifested in the spectra corresponds to the inverse of time delay t_d between two beams. The depth of the modulation represents the degree of coherence (=phase stability) between the two beams. These interference patterns are fairly stable over tens of minutes. The apparatus can be used reliably for the interferometric experiments. The inset shows an in-phase and an anti-phase interference at a specific time delay. Note that the modulation interval is the same but the relative phase of modulation is different between in-phase and anti-phase spectra.

Excitation wavelengths in phase-locked double-pulse experiments were chosen at around 414 nm near the monomer S_1 origin, since our laser system was most stable at that wavelength.

3. Experimental Results

Figure 4 displays steady-state absorption (fluorescence−excitation) and emission (fluorescence) spectra of DTA in THF solution (a) and in powder (b). Every spectrum was recorded

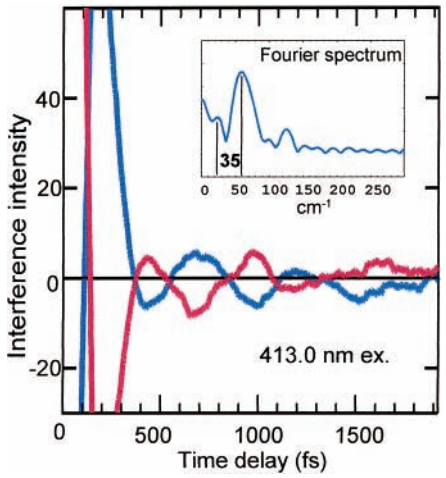

Figure 5. Fluorescence−interference (proportional to E_1E_2) curves obtained at 413.0 nm excitation. Blue and red lines are in-phase ($\phi = 0$) and anti-phase ($\phi = \pi$) signals, respectively.

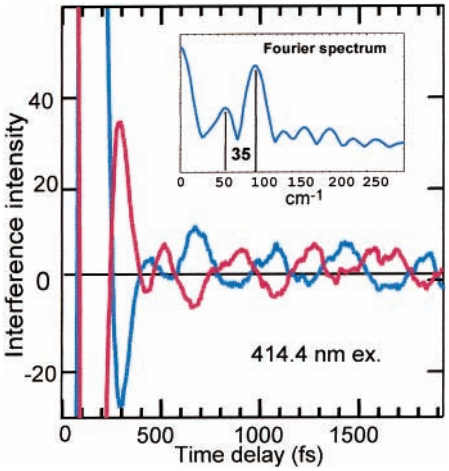

Figure 6. Fluorescence−interference (proportional to E_1E_2) curves obtained at 414.4 nm excitation. Blue and red lines are in-phase ($\phi = 0$) and anti-phase ($\phi = \pi$) signals, respectively.

at room temperature. The absorption band of DTA in solution was similar in shape to the anthracene monomer with the S_1 origin at 408 nm and S_3 origin at 280 nm. The peaks due to vibrational progressions in the S_1 manifold were observed at 367 and 385 nm. The fluorescence spectra both in solution and in powder exhibited only a diffuse and broad band, which was different obviously from the mirror image of the absorption profile in solution. Our previous picosecond time-resolved fluorescence study[5] has shown that structured fluorescence appears in the 0−25 ps range, while the diffuse broad band, which has the same profile as the steady-state fluorescence, appears after 50 ps. Thus, the broad fluorescence band has been assigned as interchromophore excimer formation.

The absorption band of DTA powder is significantly broadened in comparison with the solution absorption band and is a mirror image of the powder fluorescence spectrum. This broadening of the powder absorption band might be due to the formation of H- and J-aggregates as suggested by Cano et al.[24] for perylene derivative [bis(neopentylimido)perylene] films on glass plate.

Figures 5 and 6 display in-phase ($\phi = 0$) and anti-phase ($\phi = \pi$) fluorescence−interference (proportional to E_1E_2) curves, which were obtained through lock-in detection referenced to $f_1 + f_2$, plotted against a time delay between phase-locked pulse pairs excited at 413.0 nm (Figure 5) and at 414.4 nm (Figure

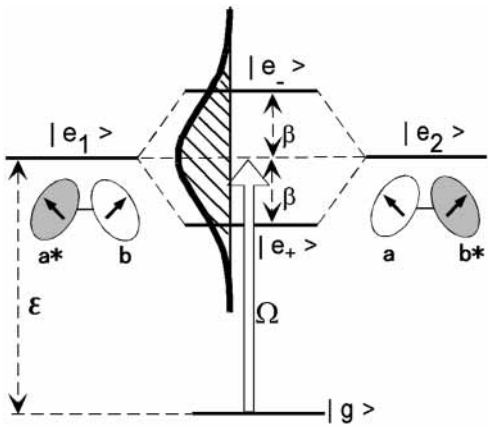

Figure 7. Three-level model system used for calculations. Locally excited states ($|e_1\rangle$ and $|e_2\rangle$) of two identical chromophores interact each other to form molecular eigenstates $|e_+\rangle$ and $|e_-\rangle$.

6), respectively. At both locking wavelengths, quantum beats having two frequency components were observed as shown in the Fourier power spectra in insets. The beat patterns between the in-phase (enhanced) and the anti-phase (depreciated) curves are symmetric with respect to the zero signal-intensity line. The beat intensity decayed with a time constant of ~1.2 ps attributable to the pure dephasing time constant T_2' between the two eigenstates composed of degenerated chromophore levels. The frequencies of quantum beats varied with locking wavelength, though no significant emission-wavelength dependence was observed. The low-frequency components were observed at 25 and 60 cm^{-1} at 413.0-nm excitation, and at 65 and 100 cm^{-1} for 414.4-nm excitation. Note that the difference of two frequency components has the common value of 35 cm^{-1}. This experimental fact may be explained as due to a beat between the detuning of the locking frequency from the electronic transition energy and the molecular energy splitting as described in the following sections.

4. Theory

Figure 7 illustrates a scheme of a three-level system where the degenerated locally excited states ($|e_1\rangle$ and $|e_2\rangle$) of two identical chromophores interact with each other, forming molecular eigenstates $|e_+\rangle$ and $|e_-\rangle$, satisfying the condition

$$|e_\pm\rangle = \frac{1}{\sqrt{2}}(|e_1\rangle \pm |e_2\rangle) \tag{1}$$

The molecular Hamiltonian for this system is

$$\begin{aligned} H &= H_1 + H_2 + V_M \\ &= E_g|g\rangle\langle g| + (E_g + \epsilon - \beta)|e_+\rangle\langle e_+| + \\ &\qquad (E_g + \epsilon + \beta)|e_-\rangle\langle e_-| \end{aligned} \tag{2}$$

where $H_{1,2}$ and V_M are chromophore Hamiltonians and Coulombic resonance interaction between chromophores. E_g and ϵ are the energy of electronic ground state $|g\rangle$ and the transition energy between $|g\rangle$ and $|e_{1,2}\rangle$; β is the interaction matrix between $|e_1\rangle$ and $|e_2\rangle$. 2β also stands for the energy splitting between $|e_+\rangle$ and $|e_-\rangle$.

The locally excited states $|e_{1,2}\rangle$ satisfy the equation

$$H_j|e_j\rangle = (E_g + \epsilon)|e_j\rangle \qquad (j = 1, 2) \tag{3}$$

The transition dipole moment operator is assumed to be

$$\mu = \mu_{eg}(|e_1\rangle\langle g| + |g\rangle\langle e_1|) \tag{4}$$

where we neglected the doubly excited state.[15]

The interaction between the molecule and the laser field $E(t)$ is given by

$$V(t) = -\mu E(t) \tag{5}$$

$E(t)$ is assumed to be a sum of two Gaussian pulses:

$$E(t) = E_1(t) + E_2(t) \tag{6}$$

$$E_1(t) = E_0 \exp\lfloor -t^2/2\tau^2 \rfloor \cos(\Omega t) \tag{7}$$

$$E_2(t) = E_0 \exp\lfloor -(t - t_d)^2/2\tau^2 \rfloor \cos(\Omega t + \phi) \tag{8}$$

where Ω is the center frequency of the laser and τ and ϕ are the time delay and the phase angle between the laser pulses. We adopted the conventional definition of phase,[15,16] since many optical cycles are included in a femtosecond pulse (~50 fs) used in our experiment. The initial state of the system at $t = 0$ is

$$|\psi(0)\rangle = |g\rangle \tag{9}$$

We define a time evolution operator under the photon-field-free condition, U_t^{free}, as

$$U_t^{free} = \exp[-iHt/\hbar] = U_0(t, 0) \tag{10}$$

The wave function at a time t is then given by

$$|\psi(t, t_d)\rangle = U_{t-t_d-d}^{free} W_2 U_{t_d-2\delta}^{free} W_1 |g\rangle \tag{11}$$

where $W_j (j = 1, 2)$ is the time evolution operator with the laser field on, given by

$$\begin{aligned} W_j &= U_0(t_j + \delta, t_j - \delta)\left(1 - \frac{1}{i\hbar}\int_{t_j-\delta}^{t_j+\delta} dt'\, U_{t_j-t'}^{free} \mu E_j(t') U_{t'-t_j}^{free}\right) \\ &= U_{2\delta}^{free}\left(1 - \frac{1}{i\hbar}\int_{t_j-\delta}^{t_j+\delta} dt'\, U_{t_j-t'}^{free} \mu E_j(t') U_{t'-t_j}^{free}\right) \\ &\equiv U_{2\delta}^{free}\left(1 + \frac{i}{\hbar}F_j\right) \end{aligned} \tag{12}$$

$$F_j = \int_{t_j-\delta}^{t_j+\delta} dt'\, U_{t_j-t'}^{free} \mu E_j(t') U_{t'-t_j}^{free} \tag{13}$$

to the first order in the laser field. Substitution of eq 12 into eq 11 yields

$$|\psi(t, t_d)\rangle = U_\delta^{free}\left(U_t^{free} + \frac{i}{\hbar}U_t^{free} F_1 + \frac{i}{\hbar}U_{t-t_d}^{free} F_2 U_{t_d}^{free}\right)|g\rangle \tag{14}$$

Hereafter we neglect the overall phase factor U_δ^{free} in eq 14 since it gives no effect in the final result.

We neglect effects of molecular rotation and random orientations to make the discussion simple and will consider only a photoselected molecule in which absorption and emission take place through $|e_1\rangle$. The projection of $|\psi(t, t_d)\rangle$ onto $|e_1\rangle$ is calculated as

$$\begin{aligned} \langle e_1|\psi(t, t_d)\rangle = \left(\frac{i}{h}\right)\Bigg\{ &\left\langle e_1 \middle| \exp\left[-i\frac{Ht}{\hbar}\right] F_1 \middle| g \right\rangle + \\ &\left\langle e_1 \middle| \exp\left[-i\frac{H(t - t_d)}{\hbar}\right] F_2 \middle| g \right\rangle \exp\left[-\frac{i}{\hbar}E_g t_d\right]\Bigg\} \end{aligned} \tag{15}$$

By using a relation of eq 1, eq 15 can be rewritten as

$$\langle e_1|\psi(t, t_d)\rangle = \left(\frac{i}{\sqrt{2}h}\right)\left\{\left\langle e_+\left|\exp\left[-i\frac{Ht}{\hbar}\right]F_1\right|g\right\rangle + \left\langle e_-\left|\exp\left[-i\frac{Ht}{\hbar}\right]F_1\right|g\right\rangle\right\} + \left(\frac{i}{\sqrt{2}h}\right)\left\{\left\{\left\langle e_+\left|\exp\left[-i\frac{H(t-t_d)}{\hbar}\right]F_2\right|g\right\rangle + \left\langle e_-\left|\exp\left[-i\frac{H(t-t_d)}{\hbar}\right]F_2\right|g\right\rangle\right\}\exp\left[-\frac{i}{\hbar}E_g t_d\right]\right\} \quad (16)$$

The matrix element, $\langle e_+|F_j|g\rangle$, is calculated to be

$$\langle e_+|F_j|g\rangle = \langle e_+|\int_{t_j-\delta}^{t_j+\delta} dt'\, U_{t_j-t'}\mu E_j(t')U_{t'-t_j}|g\rangle$$

$$= \int_{t_j-\delta}^{t_j+\delta} dt'\, \langle e_+|U_{t_j-t'}(|e_1\rangle\langle g| + |g\rangle\langle e_1|)U_{t'-t_j}\mu_{eg}E_j(t')$$

$$\langle e_+|F_j|g\rangle = \frac{1}{\sqrt{2}}\int_{t_j-\delta}^{t_j+\delta} dt'\, \exp[i(\epsilon-\beta)(t'-t_j)/\hbar]\mu_{eg}E_j(t') \quad (16a)$$

In the same way, $\langle e_-|F_j|g\rangle$ is given by

$$\langle e_-|F_j|g\rangle = \frac{1}{\sqrt{2}}\int_{t_j-\delta}^{t_j+\delta} dt'\, \exp[i(\epsilon+\beta)(t'-t_j)/\hbar]\mu_{eg}E_j(t') \quad (16b)$$

Writing $E_j(t)$ as a sum of exponentials and rejecting the off-resonance terms (the rotating wave approximation) yields

$$\langle e_\pm|F_1|g\rangle = \frac{1}{\sqrt{2}}\mu_{eg}E_0\tau(\pi/2)^{1/2} \equiv \frac{1}{\sqrt{2}}F$$

$$\langle e_\pm|F_2|g\rangle = \frac{1}{\sqrt{2}}F\exp[-i(\Omega t_d/\hbar + \phi)] \quad (17)$$

Equation 15 is rewritten by using eq 17 and by setting $t = t_d$, at which the excitation population is measured, as follows:

$$\langle e_1|\psi(t_d, t_d)\rangle = \left(\frac{iF}{2\hbar}\right)e^{-iE_g t_d/\hbar}\{e^{-i(\epsilon-\beta)t_d/\hbar} + e^{-i(\epsilon+\beta)t_d/\hbar} + 2e^{-i(\Omega t_d/\hbar+\phi)}\} \quad (18)$$

The first and second terms of eq 18 oscillating with frequencies of $(\epsilon \pm \beta)/\hbar$ represent a time evolution of the wave packet generated by E_1. These two terms give the conventional quantum beat with a period of $T = \hbar/2\beta$ in the absence of E_2 or in the case of randomly varying ϕ. The third term represents the initial phase of the second wave packet generated by E_2 at $t = t_d$.

Equation 18 is simplified in the rigorous resonance ($\Omega = \epsilon$) case as follows:

$$\langle e_1|\psi(t_d, t_d)\rangle = \left(\frac{iF}{\hbar}\right)e^{-i(E_g+\epsilon)t_d/\hbar}\{\cos(\beta t_d/\hbar) + e^{-i\phi}\} \quad (19)$$

Population of $|e_1\rangle$ is given by

$$P(t_d, \phi) = \langle\psi(t_d, t_d)|e_1\rangle\langle e_1|\psi(t_d, t_d)\rangle$$

$$= \frac{F^2}{\hbar^2}\left\{\frac{1}{2}[\cos(2\beta t_d/\hbar) + 1] + 1 + 2\cos(\beta t_d/\hbar)\cos\phi\right\} \quad (20)$$

The term originating from E_1^2 oscillates with $2\beta/\hbar$ as mentioned above, whereas the term originating from E_1E_2, which is observed in the phase-locked pulse-pair experiments, oscillates with $\beta/\hbar$. This result is clearly interpreted as the quantum beat is caused by the interference between the wave packets produced by E_1 and E_2 in the phase-locked pulse-pair experiment. On the other hand, the conventional quantum beats observed in the fluorescence decay or time-resolved absorption measurements are due to the interference of the initial wave packet created between the molecular eigenstates $|e_\pm\rangle$. It is also clear that the interference term can be enhanced or depreciated by varying an optical phase angle ϕ.

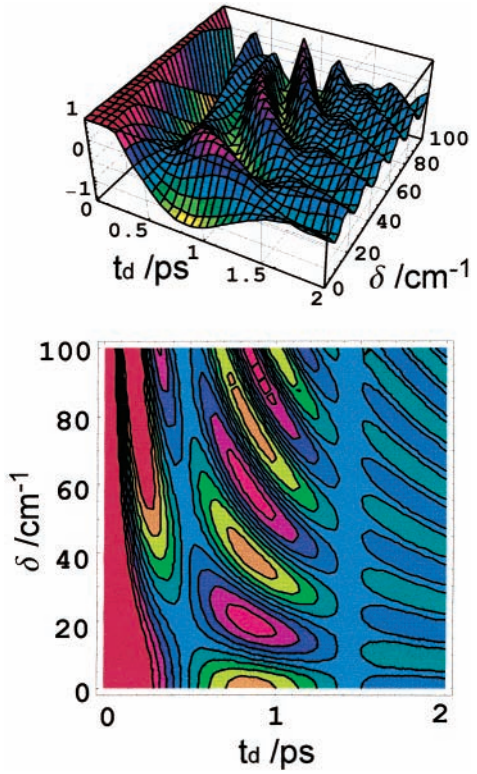

Figure 8. 3D dimensional and contour plots of time evolution of in-phase fluorescence interference signal calculated from eq 21. $2\beta = 35$ cm^{-1}; $T_2' = 1.2$ ps.

Let us consider the near resonance case, $\Omega \neq \epsilon$, in eq 18. The projection of the E_1E_2 interference term to $|e_1\rangle$ can be obtained by introducing a detuning parameter $\delta = \epsilon - \Omega$:

$$P_{int}(t_d) \propto \cos[(\delta+\beta)t_d/\hbar + \phi] + \cos[(\delta-\beta)t_d/\hbar + \phi] \quad (21)$$

In general, two frequency components are expected to be manifested in the phase-lock pulse-pair experiments, as a result of frequency modulation by detuning. The energy splitting 2β can be picked up as the difference or sum of two components of quantum beats, which remains constant when the excitation wavelength are varied. The detuning dependence of in-phase oscillatory curves is illustrated in Figure 8 indicating that the characteristic molecular-beat frequency can be modulated by the detuning.

5. Discussion

5.1. Effects of Nuclear Motion on Fluorescence Interference Signal. We have considered the effects of energy transfer in the previous sections. Nuclear motions can also affect the interference signal under phase-locked pulse-pair excitation, as first demonstrated in I_2 by Scherer et al.[15] The ground-state

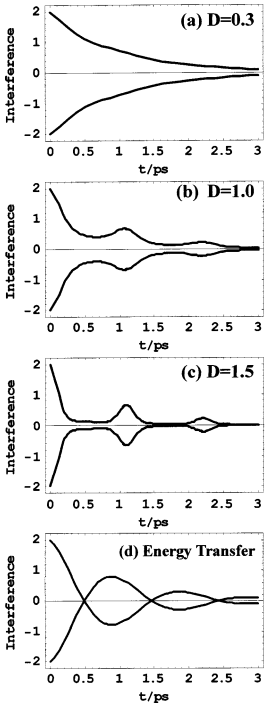

Figure 9. Vibrational coherence in the time evolution of in-phase and anti-phase fluorescence interference signal calculated from eq 22 with $\omega = 33$ cm^{-1} and $T_2' = 1$ ps in the resonant case: (a) $D = 0.3$; (b) $D = 1.0$; (c) $D = 1.5$. Curve d shows the energy-transfer coherence with $2\beta = 33$ cm^{-1} in rigorous resonance calculated from eq 21 for comparison.

vibrational wave packet starts the pendulum motion on the excited electronic potential surface, which is displaced by D from the ground electronic surface, when the molecule is photoexcited by the first laser pulse. The first wave packet interferes with the second wave packet generated by the phase-locked second laser pulse. The fluorescence interference signal in this model has been presented by Scherer et al.[15] as follows:

$$P(t_d, \phi) = \langle\psi(t_d)|e\rangle\langle e|\psi(t_d)\rangle = \frac{F_2}{\hbar^2}\left\{2 + 2\mathrm{Re}\left[\exp\left[i\left(\frac{(\Omega + \omega/2)}{\hbar} + \phi\right)\right] \times \langle 0_g|\exp[-iH_e t_d/\hbar]|0_g\rangle\right]\right\} \quad (22)$$

where ω is the vibrational frequency and $|0_g\rangle$ is the ground-state harmonic-oscillator wave function with vibrational quantum $n = 0$.

Figure 9 panels a∼c show the potential displacement (D) dependence of the vibrational coherence in the time evolution of in-phase and anti-phase fluorescence interference signals calculated from eq 22 with $\omega = 33$ cm^{-1} and $T_2' = 1$ ps in the resonant case. Curve d in Figure 6 shows the energy-transfer coherence calculated from eq 21 for comparison. The quantum beat due to the nuclear motion is negligible when D is small but becomes discernible as D increases. The quantum beats due to the nuclear vibration cannot be represented by the simple trigonometric functions, and the in-phase and anti-phase signals never cross each other. These properties are remarkably different from the energy-transfer quantum beats and would help to distinguish the energy transfer beats from the nuclear motional beats.

The in-phase and anti-phase signals, which were obtained experimentally, cross each other clearly in Figures 5 and 6, suggesting that the observed beats are not caused by the vibrational motion but rather caused by the energy transfer between chromophores. This assignment is not conclusive only from this experiment, since the detuning effect in the nuclear motional beats is not taken into consideration. However, this assignment agrees with that concluded from the fluorescence anisotropy experiment.[5] The two peak intensities should be the same in the Fourier spectrum on the basis of the theory derived above, although the observed peak intensities are different. The reason for this discrepancy remains unclear but might be due to the inhomogeneity of the sample.

TABLE 1: Apparent Energy Splitting Δ, Dephasing Constant T_2', and Corrected Interaction Energy 2β of DTA in Comparison with Binaphthyl

molecules	Δ (cm^{-1})	T_2' (ps)	2β (cm^{-1})	$2\beta T_2'/\hbar$
DTA (powder, 10 K)[a]	35 ± 11	1.4 ± 0.4	35 ± 11	9.3 ± 0.4
DTA (THF, RT)[b]	28	1.0	29	5.5
DTA (calcd)[b]			40	
binaphthyl (CCl_4, RT)[c]	28	0.2	40	1.4

[a] This work. [b] Reference 5. [c] Reference 2.

5.2. Coupling Strength in DTA. In the preceding sections we neglected the effects of dephasing on the beat frequency. In the presence of T_2', the time evolution of the system under the photon-field-free condition can be expressed by the Bloch equation:[2,3]

$$\Delta\ddot{n} + \left(\frac{1}{T_1} + \frac{2}{T_2}\right)\Delta\dot{n} + \left(4\left(\frac{\beta}{\hbar}\right)^2 + \frac{2}{T_1 T_2}\right)\Delta n = 0 \quad (23)$$

where $\Delta n = |e_1\rangle\langle e_1| - |e_2\rangle\langle e_2|$ is a population difference between the local excited states; β is the interaction matrix between the local-excited states; population decay time T_1 and dephasing times T_2 are related by $1/T_2 = 1/(2T_1) + 1/T_2'$, where T_2' is the pure dephasing time. The oscillatory behavior of Δn is manifested when the pure dephasing time T_2' is longer than $\hbar/\beta$, that is, $\beta T_2' > \hbar$. The solution of eq 23 in this case is given by

$$\Delta n(t) = \exp\left[-\left(\frac{1}{T_1} + \frac{1}{T_2'}\right)t\right]\cos(\Delta t - b) \quad (24)$$

with

$$\Delta = \sqrt{4\left(\frac{\beta}{\hbar}\right)^2 - \left(\frac{1}{T_2'}\right)^2} \quad (25)$$

where b is the initial phase. The energy splitting 2β is obtained from the apparent beat frequency Δ and T_2' by eq 25. In Table 1, the values of Δ and 2β of DTA obtained in this experiment are summarized and compared with the previous results of anisotropy experiments[2,5] and calculations.[5] The interaction energy for DTA has been calculated as $2\beta = 40$ cm^{-1} previously[5] by assuming the X-ray crystallographic structure and the dipole−dipole interaction between chromophores. The energy splitting of $2\beta = 35$ cm^{-1} obtained in this experiment is in closer agreement with the calculated value than the $2\beta = 29$ cm^{-1} obtained from the anisotropy experiment in solution. This increase in coupling strength might be explained by the fact that the aggregate structure in polycrystalline powder is more similar to the X-ray crystallographic structure used in the energy calculation.

6. Summary

The intramolecular electronic excitation coherence in dithiaanthracenophane (DTA) powder at 10 K created by the first

laser pulse has been enhanced or depreciated by the second laser pulse, which is phase-locked in the first pulse. Two anthracene rings are stacked parallel but with nearly orthogonal orientation in DTA. The interference intensity of fluorescence from DTA was enhanced or depreciated by changing a relative optical phase angle between 0° (in-phase) and 180° (anti-phase). There appeared two components of dumped oscillations in the sub-picosecond region as a function of the time delay, though the time periods varied with the excitation wavelength. On the basis of theoretical analysis, the two oscillating components have been assigned to the sum and difference between the energy separation of molecular eigenstates and the detuning frequency of the laser frequency relative to the molecular electronic transition energy.

Acknowledgment. This work is supported by Grants-in-Aid for Scientific Research (11223203 and 14540461) from the Ministry of Education, Science, Sports, and Culture of Japan.

References and Notes

(1) Kim, Y. P.; Share, P.; Pereira, M.; Sarisky, M.; Hochstrasser, R. M. *J. Chem. Phys*. **1989**, *91*, 7557.
(2) Zhu, F.; Galli, C.; Hochstrasser, R. M. *J. Chem. Phys.* **1993**, *98*, 1042.
(3) Wynne, K.; Hochstrasser, R. M. *Chem. Phys*. **1993**, *171*, 179.
(4) Kato, T.; Fujimura, Y. *Chem. Phys.* **1996**, *202*, 95.
(5) Yamazaki, I.; Akimoto, S.; Yamazaki, T.; Sato, S.; Sakata Y. *J. Phys. Chem. A* **2002**, *106*, 2122.
(6) Vos, M. H.; Rappaport, F.; Lambry, J. Ch.; Breton, J.; Martin, J.-L. *Nature* **1993**, *363*, 320.
(7) Xie, X.; Du, M.; Mets, L.; Fleming. G. R. Time-Resolved Laser Spectroscopy in Biochemistry III. *SPIE* **1992**, *1640*, 690.
(8) Monshouwer, R.; Baltuska, A.; van Mourik, F.; van Grondelle, R. *J. Phys. Chem.* A **1998**, *102*, 4360.
(9) Novoderezhkin, V.; Monshouwer, R.; van Grondelle, R. *J. Phys. Chem. B* **2000**, *104*, 12056.
(10) Zimdars, D.; Francis, R. S.; Ferrante, C.; Fayer, R. D. *J. Chem. Phys.* **1997**, *106*, 7498.
(11) Tannor, D. J.; Rice, S. A. *J. Chem. Phys.* **1985**, *83*, 5013.
(12) Shapiro, M.; Brumer, P. *Chem. Phys. Lett.* **1986**, *126*, 541.
(13) Park, S. M.; Lu, S.-P.; Gordon, R. J. *J. Chem. Phys*. **1991**, *94*, 8622.
(14) Sugawara, M.; Fujimura, Y. *J. Chem. Phys.* **1994**, *100*, 5646.
(15) Scherer, N. F.; Carlson, R. J.; Matro, A.; Du, M.; Ruggiero, A. J.; Romero-Rochin, V.; Cina, J.-F.; Fleming, G. R.; Rice, S. A. *J. Chem. Phys.* **1991**, *95*, 1487.
(16) Albrecht, A. W.; Hybl, J. D.; Gallagher Faeder, S. M.; Jonas, D. M. *J. Chem. Phys.* **1999**, *111*, 10934.
(17) Liu, X. H.; Tsujino, K.; Abe, K. *J. Phys. Soc. Jpn*. **1999**, *68*, 71.
(18) Mitsumori, Y.; Minami, F. *J. Luminesc.* **2001**, *94*, 663.
(19) De Boeij, W. P.; Pshenichnikov, M. S.; Wiersma, D. A. *Chem. Phys. Lett*. **1995**, *247*, 264.
(20) Heberle, A. P.; Baumberg, J. J.; Kohler, K. *Phys. Rev. Lett.* **1995**, *75*, 2598.
(21) Fuji, T.; Jordan, C.; Yoda, T.; Kondo, K.; Hattori, T.; Nakatsuka, H. *Jpn. Appl. Phys.* **2000**, *39*, 3429.
(22) Sakata, Y.; Toyoda, T.; Yamazaki, T.; Yamazaki, I. *Tetrahedron Lett.* **1992**, *33*, 5077.
(23) Kuritani, M.; Sakata, Y.; Ogura, F.; Nakagawa, M. *Bull. Chem. Soc. Jpn*. **1973**, *46*, 605.
(24) Cano, D. T.; Duff, J.; Aroca, R. *Appl. Spectrosc.* **2002**, *56*, 744.